EXPERIMENTS ON A HOT PLUME BASE FLOW INTERACTION AT MACH 2

P.L. Blinde, F.F.J. Schrijer, S.J. Powell, R.M. Werner, B.W. van Oudheusden

Delft University of Technology, The Netherlands, Email: p.l.blinde@tudelft.nl

ABSTRACT

A wind tunnel model containing a solid rocket motor was tested at Mach 2 to assess the feasibility of investigating the interaction between a hot plume and a high-speed outer stream. In addition to Schlieren visualisation, the feasibility of applying PIV was explored. Recorded particle images revealed that the hot plume scatters and reflects laser light, leading to a strong deterioration of the illumination conditions in regions within and near the plume. Suitable processing of the particle images could partly compensate for this and reliable velocity measurements could be obtained in directly illuminated regions. In regions near the base and below the plume, velocity measurements could still be obtained but were considered to be of lower quality. No reliable velocity measurements could be obtained within the plume itself.

1. INTRODUCTION

One of the critical areas in the design of launchers is the modelling of the complex flow that occurs in the base region during the ascent phase. The relatively low pressure in this separated flow region contributes to the overall drag of the vehicle. In addition, the unsteady interaction between the propulsive jet, the separated base flow and the external flow gives rise to fluctuating pressure loads on nearby structural elements such as the nozzle. Furthermore due to the entrainment of hot gasses, significant heat loads may occur.

In order to improve the understanding of the complex flow dynamics in the base region experimental and computational investigation are carried out. In wind tunnel experiments, the presence of an exhaust plume has often been simulated by means of a cold plume (e.g. [2–8]), generated by feeding pressurised gas to the wind tunnel model. Notwithstanding the possibility to use gases with different specific heat ratios (γ) and gas constants (R), only a limited similarity with a hot plume can be achieved [1]. Others have therefore performed experiments with actual hot plumes. Due to the practical challenges involved with generating hot jets in wind tunnels, such experimental investigations have however been rare. Examples include Musial et al. [9] who tested four 500-pound-thrust fuel-liquid-oxygen rocket motors installed in the base of a 12-inch-diameter cylindrical model at free stream Mach numbers (M_∞) ranging from 2.0 to 3.5. Peters [10][11] investigated isolated nozzle/afterbody configurations utilizing an air/ethylene burner to produce gas temperatures up to 1830 K at free stream Mach numbers from 0.6 to 1.5. Zapryagaev et al. [12] introduced a 800 K plume generated by hydrogen-fuelled combustion in a Mach 2 flow and recently Stephan et al. [13] tested a jet simulation facility in a Ludwieg tube that was shown to be capable of generating a jet with a total temperature of 620 K and a total pressure of 16 bar using heated, pressurised gas.

The measurement techniques used in previous studies included surface and field measurements using pressure probes as well as Schlieren flow visualisations. A promising addition to these measurement techniques is particle image velocimetry (PIV), which is capable of delivering a detailed experimental characterization of the flow in terms of ensembles of instantaneous velocity fields, in an efficient and non-intrusive manner [14–16]. PIV has already been successfully applied in the investigation of supersonic base flows with cold plumes (e.g. [5]). To the authors' knowledge it has however not been used in the combination of hot plumes with high-speed external flow. Using PIV in a high-speed flow facility in the presence of a hot plume requires overcoming a number of specific technical challenges, in particular creating suitable illumination and flow seeding conditions. The current study therefore aims to characterise these challenges and to assess the feasibility of using PIV to investigate the interaction between a hot plume and a transonic or supersonic outer stream.

A hot plume can be generated by using pressurised hot gas or with liquid, solid (or hybrid) propellants in a gas generator [1]. Experimental arrangements with hot plumes generated by hot gas or fuel supplied from outside the model offer the prospect of steady, controllable measurement conditions. The required gas or fuel feeding system however makes such test setups technically challenging to develop. When using solid propellants on the other hand, all the propellants are stored inside the combustion chamber leading to a far less complex arrangement. This has motivated the use of a rocket motor with a solid propellant for the current study.

2. EXPERIMENTAL ARRANGEMENTS

2.1. Facility and Experimental Conditions

The experiments have been performed in the transonic-supersonic wind tunnel (TST-27) of the High-Speed Aerodynamics Laboratories at Delft University of

Technology. The facility generates flows in the Mach number range 0.5–4.2, in a test section of dimensions 280 mm (width) × 270 mm (height). Hot-wire anemometry measurements performed in the test section found a turbulence intensity of approximately 0.5% U_∞ (based on [17]). In the present experiments, the wind tunnel is operated at a free stream Mach number (M_∞) of 2.0, a total pressure (P_0) of 2.0×10^5 N m^{-2}, and a total temperature (T_0) of 278 K. From these conditions, the free stream velocity (U_∞) is estimated to be 512 m s^{-1} using the isentropic flow relations. The Reynolds number based on the model diameter (Re_D) is 3.3×10^6.

2.2. Rocket Motor

The wind tunnel model is shown in Fig. 1. The model has a length of 483.5 mm and a diameter of 50 mm. It is mounted on a sting that is held from the back. The aft part of the model contains the solid rocket motor.

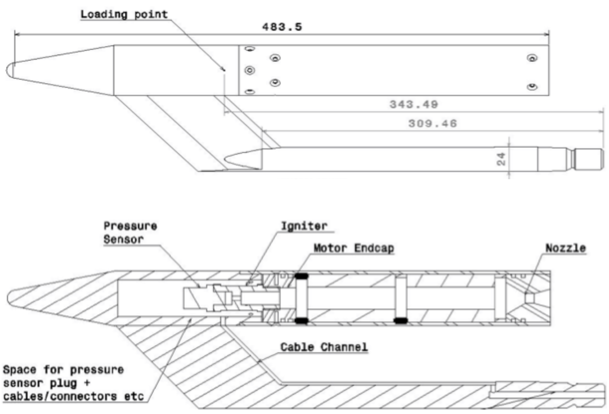

Figure 1. Schematic of the wind tunnel model including the rocket motor

The propellant, Kalinidex, is a mixture of KNO_3 - Sorbitol with a 65 - 35 mass ratio. Two propellant grains of 125 grams each are used in a Bates grain configuration. This configuration is used in order to achieve an approximately neutral burn curve as well as the desired combustion chamber pressure. The burn time of the motor is approximately 2.5 seconds. Experiments outside the wind tunnel found maximum pressures in the combustion chamber varying between 9 and 10.5 bar. The temperature in the combustion chamber was calculated to be about 1550 K based on chemical equilibrium models. The combustion gases exit through a 15° conical nozzle with a throat diameter of 9.2 mm and an exit diameter of 17 mm, yielding an area ratio of 3.4, which results in an exit Mach number of 2.4. The exit pressure is 0.64 bar, which means that the flow is under-expanded considering that the static pressure in the free stream is 0.25 bar. The presence of an under-expanded jet is typical of launchers at higher altitudes with relatively low atmospheric pressures. The motor is ignited using a pyrotechnic igniter, consisting of a squib supported by 2.5 grams of blackpowder and 0.5 grams of Ti powder. The grains were coated with a pyrogen ($Ti+KNO_3$, a binder and some charcoal) and sprinkled with rough blackpowder to further ease ignition. A diagram of aluminium tape is placed at the nozzle exit to further aid ignition. In early tests, the igniter was housed inside a steel housing as shown in Fig. 1. Several misfires occurred with this design and the current experiment uses a consumable igniter placed inside the forward propellant grain.

2.3. Schlieren Visualisation

The flow is visualized using a z-type Schlieren setup with a continuous light source, a pinhole size of 2 mm and a vertically oriented Schlieren knife. Recording is performed using a Photron FastCam SA1.1 camera operating at 500 Hz with an exposure time of 2 ms. An image without flow is subtracted from all obtained images to correct for any non-uniformity of the background and scratches in the Schlieren windows. A mask is applied to increase the contrast between the model and image frame and the flow.

2.4. Planar PIV

PIV is used to obtain velocity fields in a streamwise oriented plane downstream of the model with a size of 125 × 125 mm^2 (2.5D × 2.5D) (see Fig. 2). To assess the impact of the hot plume on the flow field, runs with and without the presence of the hot plume are recorded.

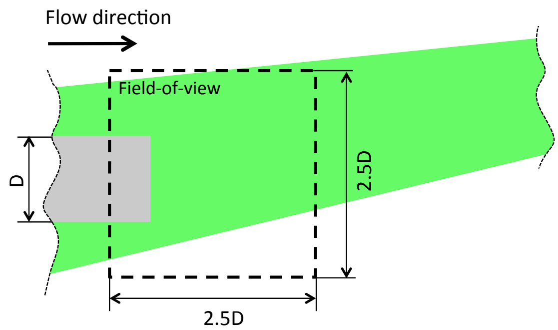

Figure 2. Location of field-of-view (black-dashed line), model (grey) and laser sheet (green)

The flow in the wind tunnel is seeded with titanium dioxide (TiO_2) particles of the type Kemira P580 having a primary crystal size of 30 nm (the actual particles form agglomerates of approximately 500 nm), a nominal density of 150 kg m^{-3} and a particle response time (τ_p) of 2.56 μs [18]. The particles are introduced by a seeding rake placed in the settling chamber, which is connected to a cyclone seeding generator.

The seeded flow is illuminated by a Quantronix Darwin Duo Nd:YLF laser (maximum pulse energy 25 mJ at 1 kHz, wavelength 527 nm, typical pulse duration 190 ns). Laser light access into the tunnel is provided by a laser probe inserted downstream of the test section [19]. The laser beam is shaped into a sheet using optics inside the probe. The light sheet thickness is approximately 1 mm.

Images are recorded by a Photron FastCam SA1.1 camera with a chip size of 1024 × 1024 pixels, 12 bit dynamic range and a pixel pitch of 20 µm. The camera is equipped with a Nikon objective of 105 mm operated at an aperture of f/4, in combination with daylight filters. The distance between the camera and the laser sheet is approximately 55 cm. The resulting digital resolution is approximately 8.5 pixels mm^{-1}.

Both the cameras and the laser are connected to a computer with a LaVision programmable timing unit (PTU) to provide for the digital synchronization. DaVis 8.1.2 software is used to control the PTU. Image pairs are acquired at a frequency of 300 Hz with a laser pulse time separation of 3 µs, which results in a particle displacement corresponding to the free stream velocity of about 11 pixels (1.4 mm). In view of the applied data acquisition rate, the subsequent instantaneous velocity measurements are uncorrelated in time.

The particle image recordings are processed with DaVis 8.1.4 software. Scattering of laser light by the plume leads to local saturation of pixels and high intensity gradients within images. Particles images are therefore pre-processed by subtracting the minimum intensity in the surrounding 5 snapshots, by disabling all saturated pixels and by normalising intensities by a min-max filter having a 6 × 6 kernel. Velocity vector fields are obtained by direct cross-correlation of the images using a multi-grid approach with window deformation. The final window size is 16 × 16 pixels for the case without plume and 24 × 24 pixels for the case with plume. With a 50% overlap, this leads to a vector pitch of 1.0 mm (8 pixels) and 1.5 mm (12 pixels) for the case without and with plume, respectively. Spurious vectors are removed using a universal median test [20] with a kernel size of 3 × 3 vectors. For the case with plume, more rigorous filtering was found to be necessary to remove spurious vectors. Any vectors with a correlation peak ratio lower than 1.25 were considered to be of insufficient quality based on visual inspection and are removed. It is noted that vectors are not replaced using linear interpolation or smoothed to enable better assessment of the feasibility of PIV under the present conditions. The quality of the particle images and resulting vector fields will be further discussed in section 3.2.

The dataset for the case without hot plume consists of 600 snapshots. For the run with hot plume a selection of 450 snapshots was made during which combustion took place and particle images of sufficient quality for PIV processing could be obtained. Of these snapshots about 75% of the resulting vector fields were found to be of sufficient quality based on visual inspection and were used for further analysis.

PIV recording parameters are summarized in Tab. 1.

Parameter	No plume	With plume
Field of view	125 × 125 mm (2.5D × 2.5D)	
Magnification	0.17	
Resolution	8.5 pixel mm^{-1}	
Window size	16 × 16 pixels	24 × 24 pixels
Vector spacing	1.0 × 1.0 mm	1.5 × 1.5 mm
Pulse separation	3 µs	
Recording rate	300 Hz	
Size of dataset	600	325

Table 1. Parameters for PIV experiment

3. RESULTS AND DISCUSSION

3.1. Schlieren Visualisation

Fig. 3 and Fig. 4 show typical Schlieren images of the flow around the model for the cases without and with plume, respectively. The flow is from left to right. The black rectangle on the left corresponds to the back of the model. The horizontal block in the lower part of the figure is a part of the sting that holds the model.

Fig. 3 for the case without plume shows a number of distinct features. The image shows an expansion fan (bright region near A) and a shear layer (thin dark line near B) on both sides of the model. Furthermore it should be noted that the compression waves at the top rear of the model (dark like near C) do not originate from the base but are the results of a reflection of the compression waves emanating from the model nose. The image also shows a compression shock (D) emanating from the model support. This shock wave can be seen to interact with the shear layer.

Fig. 4 for the case with plume clearly shows the presence of the plume. When observing the plume close to the nozzle exit, it can be seen that its diameter approximately doubles which is a clear indication that it is underexpanded (as is expected from the nozzle pressure ratio). About one model diameter downstream of the model a Mach disk is observed (E) inside the plume. In the flow surrounding the plume, similar features are observed as in the case without plume (compare Fig. 3). In addition, the image shows compression waves (F) that are generated by an outward deflection of the flow due to the expanding plume downstream of the inward deflection by the expansion over the model base. Time series of Schlieren images showed that the flow topology remains relatively stable for about 2 seconds.

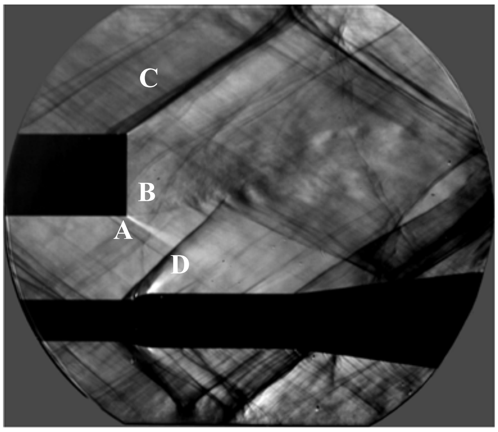

Figure 3. Schlieren image, without plume

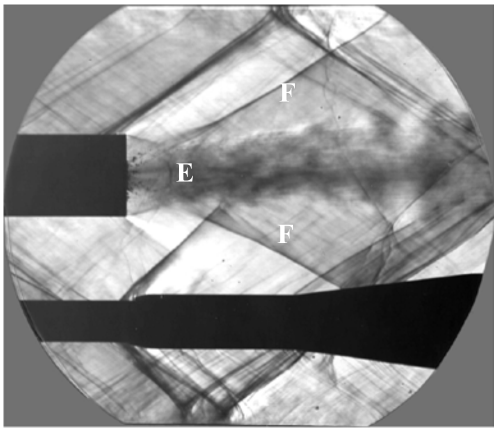

Figure 4. Schlieren image, with plume

3.2. PIV

Quality of particle images

Before presenting the resulting vector fields, first the quality of the particle images in the presence of the plume is discussed. Fig. 5 and Fig. 6 show typical particle images for the case without and with plume, respectively (flow again from left to right). Left figures depict raw images and right figures show the processed images after disabling saturated pixels, subtracting minimum intensities of surrounding snapshots and application of a min-max filter. The intensity scales are chosen such that the reflections, the plume and the particles in the surrounding flow are all visible.

Fig. 5 shows that for the case without plume, the illumination and seeding are of reasonable quality in the region of interest downstream of the model. The left figure shows an unwanted reflection from the model as well as an arc-shape reflection further downstream, originating from the wind tunnel wall. These reflections could largely be compensated for by image pre-processing (compare right and left figure), leaving only two vertical streaks at the streamwise location of the base. Note that the laser sheet does not illuminate the entire field of view (compare Fig. 2).

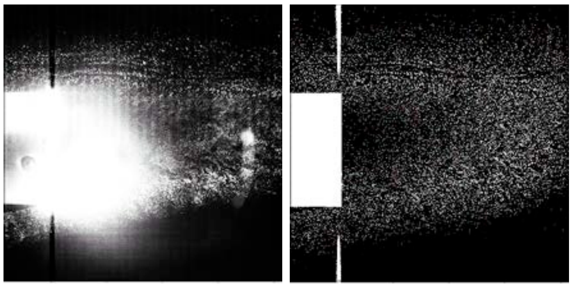

Figure 5. Particle images, no plume; Raw image (left), Processed image (right)

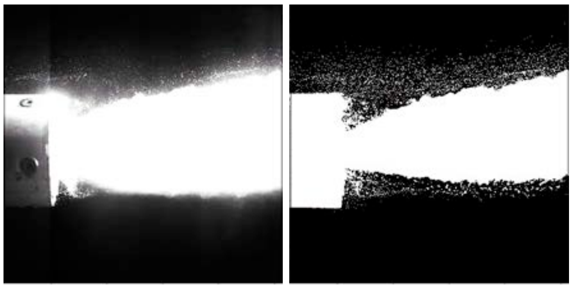

Figure 6. Particle images, with plume; Raw image (left), Processed image (right)

Especially the lower edge of the laser sheet is clearly visible. The seeding is relatively uniform downstream of the model and can be seen to decrease towards the top of the field of view. Observations of multiple snapshots showed that towards that region the seeding also becomes increasingly intermittent.

Fig. 6 shows that the quality of the particle images deteriorates drastically in the presence of the combustion plume. The plume scatters and reflects the laser light, leading to saturation and loss of contrast within the image. Fortunately, by appropriate image pre-processing these effects could partially be compensated for (compare right and left figures). The processed image (right) shows well-defined seeding particles in the region above the plume. The region directly downstream of the base and the region below the plume are characterised by the presence of bright structures and spots that are several times larger than the image of a typical seeding particle. This is attributed to the presence of large particles originating from the plume and the degradation of illumination conditions in combination with the application of a min-max filter with a relatively small kernel size. The presence of relatively large bright spots has a detrimental influence on the accuracy of the PIV measurement for a number of reasons. Where the spots represent particles in the exhaust plume, the relatively large inertia of those particles will restrict their ability to faithfully follow the flow and use them for reliable velocity measurements. Also, particles with image sizes larger than two pixels prevent accurate sub-pixel evaluation of the location of the correlation peak. Furthermore, since the spots can cover a substantial part of the interrogation window, their presence leaves less room for other particles. This effectively reduces the number of particles per window leading to an increase in the signal-to-noise ratio.

Observations of multiple snapshots showed that measurement conditions very strongly between images due to unsteadiness of the plume.

Instantaneous velocity

Fig. 7 and Fig. 8 show typical, good, instantaneous velocity fields for the case without and with plume, respectively. The snapshots correspond to the particle images shown in Fig. 5 and Fig. 6. The light region indicates the location of the model. Dark grey indicates regions in which no reliable velocity measurement could be obtained. Vectors are undersampled for clarity. The discussion in this section is limited to the quality of obtained velocity measurements.

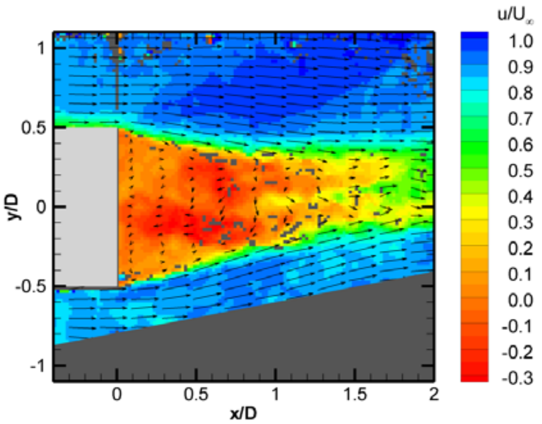

Figure 7. Typical instantaneous velocity field, no plume; vectors are undersampled by a factor 10 in x-direction and a factor 3 in y-direction

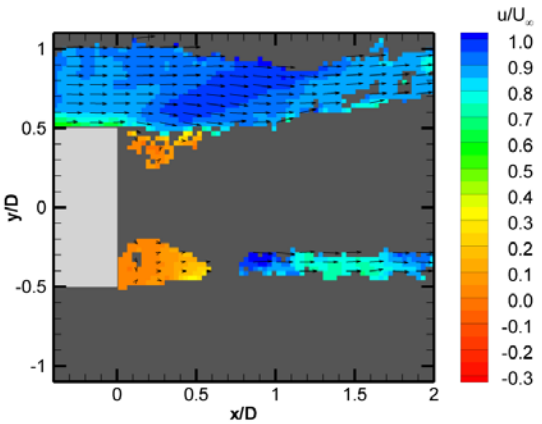

Figure 8. Typical, relatively good instantaneous velocity field, with plume; vectors are undersampled by a factor 5 in x-direction and a factor 2 in y-direction

Fig. 7 shows that for the case without plume instantaneous velocities could be obtained at almost all seeded and illuminated regions of the field of view. Only a small number of outliers has been removed by the universal median filter used for vector validation.

Fig. 8 shows that for the case with plume, velocity measurements could be obtained in a large region above the plume. These measurements are considered to be of good quality based on earlier inspection of particle images and comparison with the flow field observed from Schlieren images. This is consistent with observations from the particle images. As expected, no reliable measurements could be made within the plume. Near the edges of the plume, the correlation algorithm resulted in a large concentration of outliers, which have been removed by the applied filters for vector validation. As discussed earlier, the quality of particle images in the wake downstream of the model and below the plume further downstream was found to be low. The figure shows that velocity measurements could nevertheless be obtained in parts of these regions.

Mean velocity

Fig. 9 and Fig. 10 show the mean velocity field in the case without plume and with plume, respectively. All vectors shown are based on at least 10 instantaneous vectors. Instantaneous vectors that deviated more than three root mean squared deviations (calculated from all available instantaneous vectors at a particular location) were disregarded.

In the case without plume (see Fig. 9) a wake with a reversed-flow region can be observed downstream of the base of the model. Further downstream the velocity in the wake increases but does not recover to free-stream conditions within the field of view. Note that the wake is not perfectly axisymmetric due to compression waves in the surrounding flow coming from the model tip and support system. The flow above the wake can be seen to accelerate and turn towards the model centerline, which is consistent with the presence of an expansion fan over the model base as observed in the Schlieren image of Fig. 3. Further downstream, the flow decelerates by the compression that turns it back towards the free-stream direction. The region below the wake shows a similar but less distinct topology.

Fig. 10 shows that also in the case with plume, the flow above the plume accelerates as a result of the expansion over the model base. The subsequent deceleration and deflection away from the plume is more abrupt than in the case without plume. This is consistent with the presence of a shock wave as was inferred from the Schlieren image (see Fig. 4). Mean velocity vectors could be obtained in a small part of the wake and the region below the plume despite the low quality of the particle images in these regions.

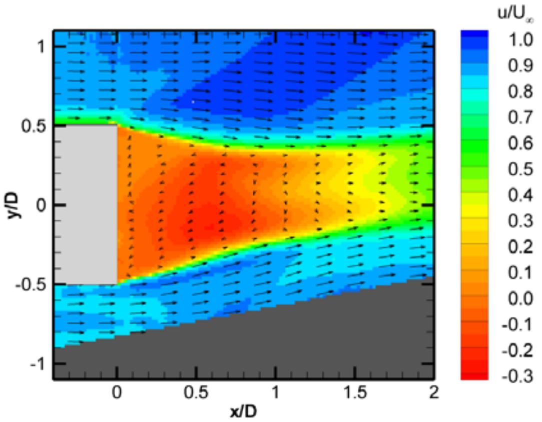

Figure 9. Mean velocity, no plume; vectors are undersampled by a factor 10 in x-direction and a factor 3 in y-direction

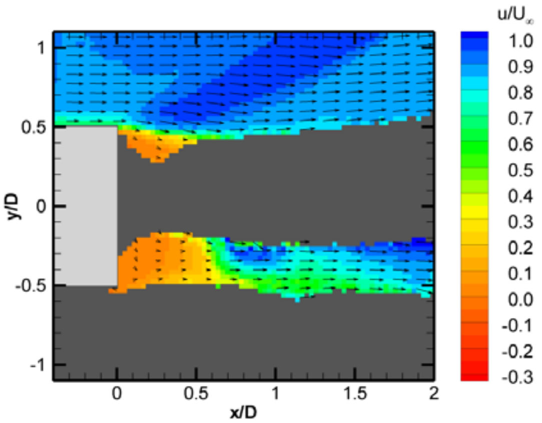

Figure 10. Mean velocity, with plume; vectors are undersampled by a factor 5 in x-direction and a factor 2 in y-direction

4. CONCLUSIONS

The current study has assessed the feasibility of applying PIV to the base flow interaction featuring a hot plume and a high-speed (supersonic) outer stream. A wind tunnel model containing a solid rocket motor was therefore tested in a conventional blowdown wind tunnel. To assess the impact of the hot plume on the flow field, runs with and without the presence of the hot plume were recorded. Schlieren visualisation was used to characterise the flow field. Particle images recorded for PIV showed that the hot plume scatters and reflects the laser light, leading to strong deterioration of the illumination conditions in regions within and near the plume. Suitable processing of the particle images could partly compensate this. Velocity measurements in the region above the plume, which is illuminated directly, were considered to be of good quality based on inspection of the particle images and vector validation. In regions near the base and below the plume, the particle images are characterised by bright spots larger than the seeding particles. The presence of these spots was linked to degradation of the PIV measurements. Whereas instantaneous and mean velocity measurements could still be obtained, they were therefore considered to be of lower quality than typical PIV measurements. No reliable velocity measurements could be obtained within the plume itself. Stringent filtering was needed to remove spurious vectors.

5. ACKNOWLEDGEMENTS

This work constitutes a cooperation between the Aerodynamics Group of the Delft University of Technology, Faculty of Aerospace Engineering and Delft Aerospace Rocket Engineering (DARE). Special thanks goes to the technicians and safety personnel of the Windtunnel Laboratories for their special dedication to this project, in particular Henk-Jan Siemer, Frits Donker Duyvis and Peter Duijndam.

6. REFERENCES

1. Schoones, M.M.J., Bannink, W.J. & Houtman E. M. (1998). *Base Flow and Exhaust Plume Interaction: Experimental and Computational Studies*. Delft University Press

2. Reijasse, P., Delery, J. (1994). *Investigation of the Flow past the ARIANE 5 Launcher Afterbody.* Journal of Spacecraft and Rockets 31(2), pp. 208-214

3. Reijasse, P., Corbel, B. & Délery, J. (1997). *Flow confluence past a jet-on axisymmetric afterbody.* Journal of Spacecraft and Rockets. 34(5), pp. 593-601.

4. van Oudheusden, B.W. & Scarano, F. (2008). *PIV Investigation of Supersonic Base-Flow–Plume Interaction*. Particle Image Velocimetry, Topics Applied Physics, 112, Springer Verlag

5. Morris, N., Buttsworth, J. & Brescianini, C., Jones, T. (1995). *An experimental and computational study of moderately under-expanded rocket exhaust plumes in a co-flowing hypersonic free stream.* In Proc. 6th International Aerospace Planes and Hypersonics Technologies Conference, AIAA Paper 95-6127

6. Bannink, W.J., Houtman, E.M. & Bakker, P.G. (1998). *Base flow/underexpanded exhaust plume interaction in a supersonic external flow.* In Proc. 8th AIAA International Space Planes and

Hypersonic Systems and Technologies Conference, AIAA Paper 98-1598

7. Kumar, R., Viswanath, P. & Prabhu, A. (2002). *Mean and fluctuating pressure in boat-tail separated flows at transonic speeds*. Journal of Spacecraft and Rockets. 39(3), pp. 430-438

8. Pindzola, M. (1963). *Jet simulation in ground test facilities.* AGARDograph. 79

9. Musial, N.T. & Ward, J.J. (1961). *Base Flow Characteristics for Several Four-Clustered Rocket Configurations at Mach Numbers from 2.0 to 3.5.* NASA TND-1063.

10. Peters, W.L. (1976). *An evaluation of jet simulation parameters for nozzle afterbody testing at transonic Mach numbers*. 17th Aerospace Sciences Meeting, AIAA paper 77-106.

11. Peters, W.L. (1979). *Jet simulation techniques: Simulation of temperature effects by altering gas composition*. 17th Aerospace Sciences Meeting, AIAA paper 79-327.

12. Zapryagaev, V., Lokotko, A.V., Nikiforov, S.V., Pavlov, A.A., Tchernyshev, A.V., Bannink, W.J. & Muylaert, J. (2002). *Experimental Investigation of Base Pressure with Hot Supersonic Jet for External Supersonic Flow.* In Proc. 4th Symposium on Aerothermodynamics for Space Vehicles, Capua ,Italy

13. Stephan, S., Radespiel, R.& Müller-Eigner, R. (2013). *Jet Simulation Facility using the Ludwieg Tube Principle*. In Proc. 5th European Conference for Aeronautics and Space Sciences (EUCASS)

14. Raffel, M., Willert, C., Wereley S. & Kompenhans, J. (2007). *Particle Image Velocimetry, a practical guide. 2nd editon.* Springer, Berlin

15. Adrian, R.J. & Westerweel, J. (2011). *Particle image velocimetry*. Cambridge University Press

16. Adrian, R.J. (2005). *Twenty years of particle image velocimetry*. Experiments in Fluids (39), pp. 159-169

17. Giepman, R.H.M., Schrijer, F.F.J. & van Oudheusden, B.W. (2014). *High-resolution PIV measurements of a transitional shock wave-boundary layer interaction*. In Proc. 44th AIAA Fluid Dynamics Conference

18. Ragni, D., Schrijer, F.F.J, van Oudheusden, B.W. & Scarano, F. (2010). *Particle tracer response across shocks measured by PIV*. Experiments in Fluids (50) pp. 53–64

19. Donker Duyvis, F.J. (2005). *Laser sheet probe design for PIV in high speed wind tunnels*. In Proc. PIVNET II International Workshop on the Application of PIV in Compressible Flows, Delft, the Netherlands

20. Westerweel, J. & Scarano, F. (2005). *Universal outlier detection for PIV data.* Experiments in Fluids (39), pp. 1096–1100